EAST EUROPEAN JOURNAL OF PHYSICS. 2. 109-121 (2026)
DOI:10.26565/2312-4334-2026-2-10 ISSN 2312-4334

POROUS CERAMICS AND METAL HYDRIDE MATERIALS FOR EFFICIENT HYDROGEN STORAGE

M.S. Payzullakhanov[1,2], O.R. Parpiev[1], F.A. Giyasova[3], S.U. Turapova[1], E.Z. Nodirmatov[1], M.A. Yuldoshev[4]*, O.T. Ismanova[5], F.A. Giyasov[3], A. Egamberdiyev[6], S.K. Abdizhaliev[7], M.A. Jalelov[7], S.A. Tursinbaev[7], A.A. Abduvakhobov[3]

[1]*Institute of Materials Science, Academy of Sciences of the Republic of Uzbekistan, Tashkent, Uzbekistan*
[2]*Fergana State Technical University, Uzbekistan*
[3]*Kimyo International University in Tashkent, Uzbekistan*
[4]*Turan International University, Namangan, Uzbekistan*
[5]*Namangan State University, Namangan, Uzbekistan*
[6]*Tashkent Institute of Irrigation and Agricultural Mechanization Engineers, National Research University, Uzbekistan*
[7]*Nukus State Pedagogical Institute Named After Ajiniyaz, Nukus, Uzbekistan*
**Corresponding Author e-mail: murod.yuldoshev1993@gmail.com*
Received January 26, 2026; revised April 16, 2026; accepted April 17, 2026

In this work, we investigated synthesized porous aluminosilicate materials containing burnable additives, which form a single-phase cubic zeolite structure (Fm3m, a=4.056 Å). The porous ceramic with a zeolite composition at 200°C and a hydrogen pressure of 12 atm exhibited hydrogen absorption of 11 wt.%. We also studied the initial metallic lithium (BCC, a ≈ 3.507 Å), which was subjected to hydrogenation in the developed sealed reactor at 12 atm and 700 °C with the formation of LiH hydride (FCC, NaCl type, a ≈ 4.081 Å, d_{111} ≈ 2.356 Å). The average size of LiH crystallites does not exceed 100 nm, and the maximum hydrogen capacity of lithium reached 12.4 wt.%. The developed reactor enables safe, high-temperature, high-pressure hydrogenation. These data demonstrate the potential of lithium, titanium, and sodium hydrides, and porous aluminosilicates for the accumulation, storage, and transportation of hydrogen.
Keywords: *Porous aluminosilicates; Lithium hydride; Synthesis; Hydrogenation; X-ray phase analysis; Hydrogen storage; Cubic structure; Hydrogen capacity*
PACS: 68.37.Hk, 78.70.Ck, 77.84.-s

INTRODUCTION

Gaseous fuels, primarily hydrogen and methane, are currently considered among the most promising energy sources, as their use in existing power plants and engines is technically feasible and provides high efficiency [1]. Hydrogen is of particular importance in the context of developing sustainable energy systems. As the most abundant element in the universe and possessing the simplest atomic structure, it is a versatile energy carrier capable of efficiently storing and transporting energy in a form convenient for practical use. Due to its environmental friendliness, high energy density, and compatibility with renewable energy sources, hydrogen is considered a key element in the transition to low-carbon energy. The development of hydrogen energy is central to global strategies to reduce dependence on fossil fuels and minimize anthropogenic environmental impact. A significant advantage of hydrogen is its ability to enable decarbonization of sectors that are difficult to electrify, including heavy transport, industrial production, and power generation [2], making it a fundamental player in building a sustainable energy infrastructure for the future [3].

According to IHS Cambridge Energy Research Associates, the world's natural gas reserves can meet humanity's energy needs for at least 250 years [4]. However, the key factor hindering the widespread use of gas fuels, especially for autonomous and remote energy sources, remains the lack of energy-efficient, fire- and explosion-proof storage and transportation systems capable of handling high gas densities [5]. Hydrogen is of particular interest due to its high specific heat of combustion (~120 MJ kg^{-1}) and the environmental friendliness of its products [6]. However, the practical implementation of hydrogen energy is significantly limited by the difficulties of its storage. Current technologies involve compressing hydrogen to approximately 700 bars (≈70 MPa), which requires robust, sealed tanks and carries an increased risk of explosion [7]. Cryogenic storage, implemented at approximately 20 K, is associated with additional energy costs and increased engineering system complexity [8]. Therefore, the development of alternative, safer methods of hydrogen storage is one of the key objectives of hydrogen energy.

The efficient use of hydrogen in energy systems requires the development of safe, cost-effective, and high-performance storage technologies [9, 10]. One of the most promising approaches is solid-state storage, based on retaining hydrogen in solid materials in molecular or atomic form [11]. This approach is implemented through two main mechanisms: physical adsorption and chemical absorption. Physical absorption is primarily due to van der Waals interactions and is typical for materials such as porous carbon structures, metal–organic frameworks (MOFs) [12], and

Cite as: M.S. Payzullakhanov, O.R. Parpiev, F.A. Giyasova, S.U. Turapova, E.Z. Nodirmatov, M.A. Yuldoshev, O.T. Ismanova, F.A. Giyasov, A. Egamberdiyev, S.K. Abdizhaliev, M.A. Jalelov, S.A. Tursinbaev, A.A. Abduvakhobov, East Eur. J. Phys. 2, 109 (2026), https://doi.org/10.26565/2312-4334-2026-2-10
© M.S. Payzullakhanov, O.R. Parpiev, F.A. Giyasova, S.U. Turapova, E.Z. Nodirmatov, M.A. Yuldoshev, O.T. Ismanova, F.A. Giyasov, A. Egamberdiyev, S.K. Abdizhaliev, M.A. Jalelov, S.A. Tursinbaev, A.A. Abduvakhobov, 2026; CC BY 4.0 license

covalent organic frameworks (COFs) [13]. Despite the high rate and reversibility of sorption processes, this mechanism typically requires low temperatures and elevated pressures and is characterized by a relatively limited hydrogen capacity [14]. Chemical bonding involves the dissociation of hydrogen molecules, followed by the formation of hydride phases, thereby providing a higher storage density [15]. Within this approach, which includes metal and complex hydrides, hydride materials have attracted considerable attention in recent years as a promising basis for developing sustainable hydrogen storage technologies [16]. A promising area is solid-phase hydrogen storage via chemical binding in metal hydrides, which offer high storage density at relatively low pressures (1-40 bar). The volumetric density of hydrogen in metal hydride systems can reach 120-150 kg m^{-3}, which significantly exceeds the value of ~39 kg m^{-3} for compressed hydrogen at a pressure of 700 bar [17-19]. Metal hydrides are also characterized by high reversibility in hydrogen absorption and release, as well as the possibility of multiple cycles. The theoretical mass capacity of such materials is 7.6 wt.% for MgH_2, 4.04 wt.% for TiH_2 and reaches 12.7 wt.% for LiH [20, 21]. At the same time, hydrogenation processes are usually carried out at temperatures of 300–700°C and hydrogen pressures above 10–15 atm, which lead to significant energy costs and impose limitations on the kinetics of phase transformations and thermal stability [22–24].

The kinetics of hydrogen absorption in metal hydride layers are limited by coupled heat and mass transfer processes, which lead to a slow system response to refueling and reduced overall storage efficiency. For a TiMn-based metal hydride material with specified porosity and thermal conductivity parameters, three composite groups were studied: group A, containing 5 wt.% silicone gel and 5 wt.% single-wall carbon nanotubes; group B, including 5 wt.% silicone gel; and group C, containing 5 wt.% silicone gel and 5 wt.% silicone sheets [25]. It was found that the highest porosity is observed in group A (0.527), exceeding the values of other samples by approximately three times, while its thermal conductivity is minimal (2.476 $W \cdot m^{-1} \cdot K^{-1}$) compared to group B (3.189 $W \cdot m^{-1} \cdot K^{-1}$) and group C (3.246 $W \cdot m^{-1} \cdot K^{-1}$). The identified differences in the structural and thermophysical characteristics determine the features of the materials' kinetic behavior: for group A, the diffusion-limited mode of hydrogen absorption in the range of 0.5-1.15 wt.% predominates, which is associated with a well-developed macroporous structure that ensures efficient hydrogen transfer. At the same time, group C is characterized by a higher absorption rate at later stages (above 1.15 wt.%), where the key role is played by increased thermal conductivity, which determines the intensity of the heat flow and, accordingly, the driving force of the sorption process.

In recent years, porous inorganic materials have attracted considerable interest, primarily aluminosilicate and alumina-alumina ceramics, which are capable of accumulating hydrogen through a combination of physical adsorption and diffusion in a developed porous structure [26, 27]. According to the literature [28], such materials are characterized by water absorption in the range of 8-25 %, which corresponds to an open porosity of about 20-50 % and a specific surface area of up to 300-800 $m^2 \cdot g^{-1}$. An increase in the specific surface area and degree of porosity promotes an increase in hydrogen capacity, especially at temperatures above 100 °C, when the contribution of physical adsorption is supplemented by thermally activated diffusion processes [29-32]. The efficiency of hydrogen absorption of porous materials is often estimated using the aspect number, defined as the relative increase in the mass of a sample after saturation with hydrogen. For most aluminosilicate and oxide ceramics, this parameter, according to published data, does not exceed 1-6 wt.% at temperatures up to 300 °C [33, 34]. An increase in the aspect number is possible through optimization of the chemical composition, the introduction of silica-containing components, and the formation of developed open porosity using burnable additives that provide a controlled architecture of the pore space [35, 36]. Lithium hydride is of interest as a reference system for assessing the ultimate capabilities of solid-phase hydrogen storage. Lithium has one of the highest theoretical hydrogen capacities, and the formation of LiH is accompanied by a significant increase in the mass of the material. [37, 38]. X-ray diffraction analysis of lithium samples treated in a hydrogen flow at a pressure of 12 atm and a temperature of 700 °C characterizes the almost complete conversion of the original metal into lithium hydride with a cubic structure and space group $Fm\bar{3}m$, which is confirmed by the presence of intense narrow diffraction peaks and the absence of reflections of metallic lithium. The achieved hydrogen capacity is close to the theoretical limit of 12.5-12.7 wt.% [39, 40]. At the same time, such high temperatures and energy costs significantly limit the practical application of lithium hydride in hydrogen storage systems. Against this background, porous aluminosilicate ceramics, which combine a developed porous structure, controlled phase composition and the ability to operate at moderate temperatures and pressures, are considered a promising alternative to traditional metallic hydrides [41, 42]. Despite growing interest in such materials, the quantitative relationships between their chemical composition, porous structure parameters, phase state, and hydrogen absorption characteristics, especially in the temperature range of 100–200°C, remain poorly understood [43, 44]. Filling this gap represents an important scientific and applied challenge. Furthermore, conducting comprehensive analytical studies aimed at assessing their readiness for commercial implementation, taking into account market requirements, remains a pressing task. Such systematic reviews allow us to identify the most promising materials and technological solutions, as well as focus further research on addressing existing limitations and unresolved issues [45].

The aim of this work is to conduct a comprehensive study of metal hydrides as hydrogen carriers, assessing their applicability in stationary and mobile systems, determining the ultimate efficiency of solid-phase storage using the example of lithium metal hydrogenation using X-ray phase analysis, and developing and studying porous ceramic materials based on aluminum oxide and aluminosilicates to determine the influence of their composition, structure, and temperature conditions on hydrogen sorption and retention processes.

EXPERIMENTAL SAMPLES AND MEASUREMENT METHODS

During experimental studies of material synthesis, various compositions aimed at producing porous ceramics were tested. The porous ceramic materials were formed by introducing burnable additives into the ceramic matrix. The chemical composition of the starting components is presented in Table 1.

Table 1. Chemical composition of raw materials

RAW MATERIALS	Al_2O_3	Fe_2O_3	SiO_2	Na_2O	K_2O	CaO	MgO	Volatile impurities
Kaolin	36.91	2.52	46.84	0.04	0.42	0.24	0.22	12.81
Diatomite	5.65	3.38	88.23	0.34	0.87	0.62	0.82	-

Kaolin was pre-melted in a solar furnace using the previously described method [46], after which the resulting material was wet ground in a ball mill to a particle size of less than 63 μm.

Diatomite was chosen as one of the main components due to its naturally highly porous structure: total porosity reaches 92%, and the SiO_2 mass fraction ranges from 62-97%. Diatomite may also contain fine sand (up to 10%), clay minerals, and trace amounts of organic matter. Based on these components, an aluminum oxide-enriched material was developed. The raw materials used to produce the porous ceramics corresponded to the chemical composition listed in Table 2.

Table 2. Chemical composition of the initial state of the raw material

Oxide	Al_2O_3	P_2O_5	SiO_2	Na_2O	Fe_2O_3	SO_3
Content, wt.%	67.12	0.21	25.21	6.88	0.02	0.56

As shown in Table 2, the main components of the ceramic material are alumina (67 wt.%), silicon oxide (25.2 wt.%), and sodium oxide (6.9 wt.%).

The phase composition of the synthesized samples was studied by X-ray diffraction analysis using a PANalytical Empyrean diffractometer (Cu Kα radiation) in Bragg-Brentano reflection geometry at a wavelength of λ=1.5418 Å. Diffraction patterns were recorded in the angular range $20° \leq 2\theta \leq 60°$, where 2θ is the Bragg angle. The microstructure and surface morphology of the samples were studied by scanning electron microscopy (SEM) using JEOL JSM-6510 and HITACHI FLEXSEM 100 microscopes.

Hydrogenation experiments were conducted using porous zeolite-type materials and metals (aluminum, iron, magnesium, titanium, and lithium), applied in both bulk and powder form [46, 47]. The hydrogenation process was carried out in a reactor equipped with high-temperature packing, as shown in Figure 1.

The high-temperature reactor container shown (Fig. 1) is made of stainless steel and equipped with a sealed lid with a bolted clamping system. The reactor operates according to the diagram shown (Fig. 2) and is equipped with a pressure gauge, gas inlets and shutoff valves for the supply and release of working gas, and sealing devices for operation at elevated temperatures and pressures. The reaction zone is heated using an electric heating module with a digital temperature controller, allowing for precise temperature control and maintenance during hydrogenation experiments.

Figure 1. High-temperature sealed reactor for hydrogenation processes

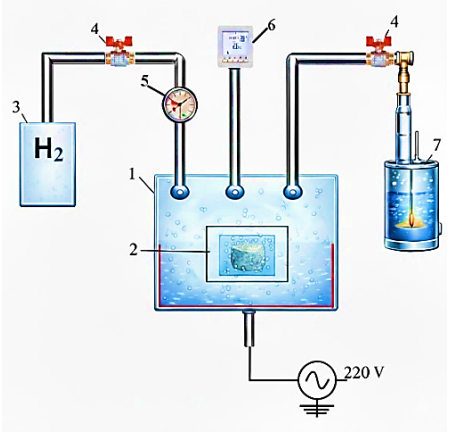

Figure 2. Schematic diagram of the furnace-reactor for hydrogenation of absorption materials at high temperatures (up to 700 °C) and hydrogen pressures up to 15 atm, including: 1 - steel furnace-reactor with an electric heating system from a 220 V network; 2 - absorber; 3 - hydrogen cylinder for feeding gas to the furnace-reactor; 4 - shut-off and control valves; 5 - pressure gauge; 6 - thermocouple connected to a temperature meter; 7 - exhaust gas reservoir

Before the experiment, the samples were dried at 200°C, then weighed and placed in the reactor. To remove air from the reaction chamber before heating, the reactor was purged with hydrogen. The reactor was then sealed and

pressurized with hydrogen at 10-15 atm. Heating was performed according to a preset temperature program ranging from 150 to 700°C. After the holding period, the reactor was cooled either slowly or rapidly, depending on the experimental conditions. Upon completion of cooling, the samples were removed and reweighed. The degree of hydrogenation was assessed by the relative weight gain:

$$\alpha=[(M-M_0)/M_0]\times 100\ \%, \quad (1)$$

where M_0 is the mass of the original sample, M is the mass after hydrogenation.

The formation of metal hydrides is a heterogeneous process [48] that involves the adsorption of molecular hydrogen on the metal surface, its dissociation to form atomic hydrogen, and subsequent diffusion of atoms into the metal's crystal lattice.

RESULTS AND DISCUSSION

Zeolites are known to have high sorption capacity and are widely used in water purification processes to remove hydrocarbon compounds. Their effectiveness is largely determined by the properties of their microstructure, where a fine-grained structure promotes increased sorption activity [49, 50]. In general, the effectiveness of adsorption processes is determined by the parameters of the porous structure and the energy characteristics of the adsorbent-adsorbate interaction, which is driving growing interest in the development of new microporous materials with a specific micropore volume of about 1-2 cm^3/g and a specific surface area of 1500-2000 m^2/g [51].

Therefore, studying the microstructural features of zeolites is of considerable interest for optimizing their performance properties [52, 53]. In particular, the microstructural features of porous ceramics of the zeolitic aluminosilicate composition Al_2SiNaO_6, studied by scanning electron microscopy, are shown in Fig. 3 at magnification ~×1000.

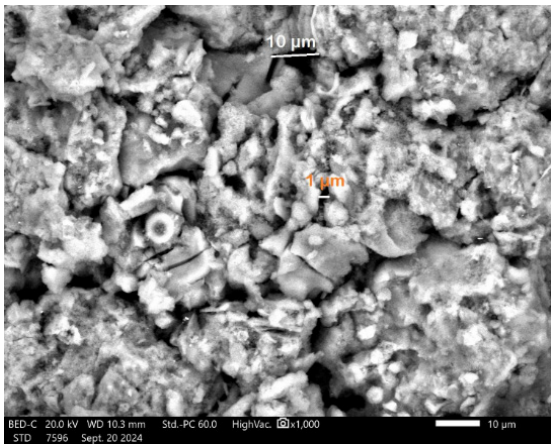

Figure 3. SEM image of the microstructure of porous ceramics of zeolitic aluminosilicate composition Al_2SiNaO_6

Image analysis shows that the material is characterized by a developed hierarchical porous structure. The sizes of the primary particles and their agglomerates are in the range of 1-10 µm, which corresponds to the scale marks in the micrograph. The intergranular space is formed by a system of open pores, predominantly micron and submicron in size (0.3–2 µm), indicating high open porosity of the material. This morphology indicates the formation of a branched pore network, ensuring efficient mass transfer of gaseous and liquid media [54–56]. The rough surface of the grains contributes to an increase in the specific surface area, which for zeolitic aluminosilicate materials, as a rule, reaches values of 100–400 m^2/g. The observed localized areas of compaction up to 5–8 µm in size may be associated with partial sintering and recrystallization of the aluminosilicate matrix during heat treatment. Moreover, the preservation of open pores indicates that the firing temperature was below the threshold for intense shrinkage and pore closure, which is an important factor for the functional properties of the material. The resulting microstructure provides a combination of mechanical cohesion of the ceramic framework and a developed internal surface area. This suggests a high adsorption capacity (approximately 0.5-2.0 mmol/g for small molecules) and the potential for the use of porous Al_2SiNaO_6 ceramics in adsorption, ion exchange, and catalysis processes, as well as in gas storage and transportation systems, including hydrogen [46, 57].

Figure 4 shows an SEM image of the porous structure of a composite absorbent based on Al<SiO_2> (aluminum powder in a silicon dioxide matrix), obtained at a magnification of ×100 for an area of 800×800 µm.

A quantitative analysis of the structure's morphology allowed us to determine the total pore number ($1.35\cdot10^3$) and record their surface concentration at $2.1\cdot10^{-3}$ pores/μm^2. The pore size distribution is characterized by pronounced heterogeneity. The average equivalent pore diameter, calculated based on the area, is 5.4 µm with a median value of 3.1 µm, confirming the presence of a pronounced distribution asymmetry and the predominance of the fine fraction in the structure. These geometric parameters significantly influence the development of the specific surface area and the intensification of capillary phenomena. The presence of pores of varying order forms a branched hierarchical network

that minimizes diffusion resistance and facilitates deep penetration of the working medium into the material. The minimum recorded size is approximately 1.2 μm, while the main range varies between 1.2 and 15 μm. Individual coarse pore formations reach d_{max}≈35 μm, which is associated with the coalescence and agglomeration of particles. An area porosity of 0.62 %, combined with a high pore density, determines the morphology of the sample's internal surface. The resulting active phase contact area increases the material's efficiency as an absorber. This porosity value is typical of materials with intense interparticle void formation. Morphological analysis reveals that the structure is hierarchically organized and includes pores at multiple scales. The predominance of pores smaller than 10 μm indicates the formation of a fine- and mesoporous structure, while the presence of individual macropores is due to localized aggregation of aluminum particles. Al particles form irregular agglomerates, between which intergranular voids form, while the binding phase SiO_2 stabilizes the framework and prevents complete compaction of the system. The obtained parameters reflect the presence of a branched but heterogeneous pore structure resulting from the agglomeration of aluminum powder and the formation of interconnected channels in the silica matrix, which significantly influences the sorption capacity and permeability of the material. The combination of high porosity, significant pore density, and a wide pore size distribution makes this material promising for use as an effective absorber [58, 59].

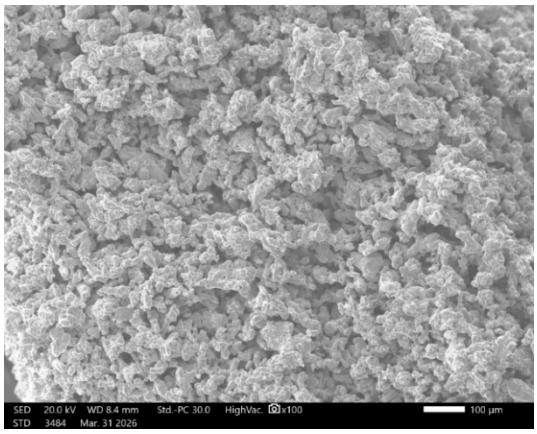

Figure 4. Surface morphology of the porous absorbing structure of Al<SiO_2>

The developed porous structure and the presence of active metal centers ensure their high reactivity with respect to hydrogen, realized through the chemisorption mechanism with the formation of strong Al-H bonds [60, 61]. The process includes the dissociative adsorption of molecular hydrogen on the aluminum surface, subsequent diffusion of atomic hydrogen and the formation of a hydride phase, including AlH_3 [61]. The efficiency of sorption increases at temperatures above 200 °C due to surface activation and increased mobility of hydrogen atoms [62]. Desorption is accompanied by the rupture of AlH bonds and occurs upon heating in the range of 200 - 400 °C [63].

Figure 5 shows the isotherms of hydrogen sorption and desorption in porous Al_2SiNaO_6 ceramics at a temperature of 200 °C in the pressure range of 1–11 atm.

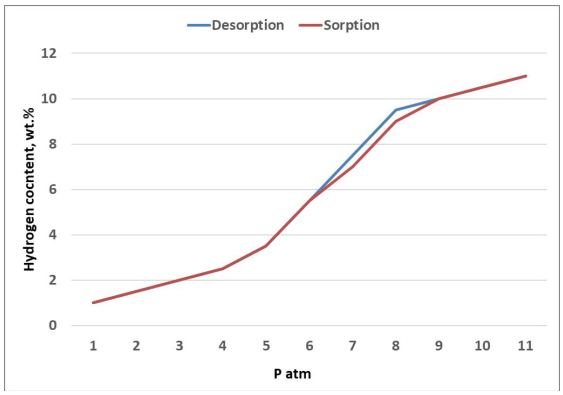

Figure 5. Isotherms of hydrogen sorption and desorption in porous ceramics Al_2SiNaO_6 at a temperature of 200°C

When analyzing the curves (Fig. 5), a gradual increase in the hydrogen content from 1 to 3.5 wt.% is observed in the low-pressure region (1-5 atm). This region corresponds to the initial stage of sorption, during which predominantly physical adsorption of hydrogen occurs on the pore surface and active sites of the material. The linear nature of the curve characterizes a relatively weak interaction and gradual saturation of available adsorption sites. In the pressure range of 5-8 atm, a sharp increase in the hydrogen content is recorded (up to 9-9.5 wt.%). This region is characterized by accelerated sorption and reflects the transition to more intense absorption mechanisms. It is likely that chemisorption occurs in this region, with the formation of chemical bonds between hydrogen and aluminum (possibly the formation of

hydride phases: AlH). Additionally, capillary condensation of hydrogen in meso- and macropores can occur, which is due to the developed porous structure of the material. With a further increase in pressure (8-11 atm), the curve reaches a plateau (10-11 wt%). The established dependence demonstrates saturation of the system with hydrogen and filling of most of the accessible pores and active sites. Reaching a plateau indicates a limited capacity of the material at a given temperature. Comparison of the sorption and desorption curves reveals hysteresis in the medium pressure range (6-9 atm): the desorption curve passes above the sorption curve. The process of hydrogen desorption from porous ceramics occurs intensively at a temperature of 200 °C, ensuring the complete release of previously absorbed hydrogen in a volume of up to 11 wt.% within 2 minutes; the material retains the ability to undergo multiple sorption and is characterized by cyclic stability within 5 sorption-desorption cycles, however, after the fifth cycle, degradation of its structure is observed, accompanied by a decrease and subsequent loss of sorption properties [60, 61, 64].

The obtained data are typical for porous materials with a developed structure and allow us to conclude the presence of pores of various sizes (micro-, meso-, and macropores), capillary effects, and hydrogen retention within the pores, as well as partially irreversible processes caused by chemisorption and the formation of hydride phases. The convergence of the sorption and desorption curves at high pressures (9-10 atm) confirms the achievement of a quasi-equilibrium state of the structure and the mitigation of the influence of kinetic limitations. The obtained isotherms demonstrate a combined mechanism of hydrogen absorption in Al_2SiNaO_6, including physical adsorption, chemisorption, and capillary condensation. Materials of this type are considered promising for the storage and accumulation of hydrogen due to reversible chemisorption and the formation of stable hydride compounds, while pronounced hysteresis indicates the presence of a developed hierarchical porous structure that facilitates the effective accumulation of gas [65, 66].

Figure 6 shows the particle size distribution spectrum for a sample of porous aluminosilicate ceramics of the composition Al_2SiNaO_6, obtained by laser diffraction.

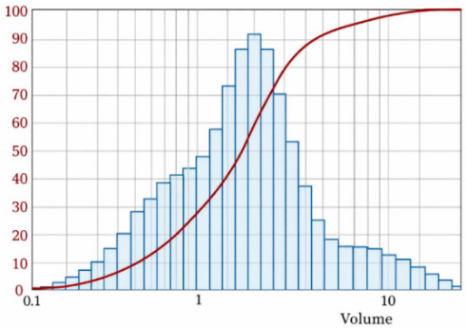

Figure 6. Spectrum of particle size distribution of a porous ceramic sample of aluminosilicate composition Al_2SiNaO_6

The distribution is polydisperse, reflecting the presence of particles of different sizes. The majority of particles are concentrated in the range of 0.5-3.0 μm, with the distribution maximum (modal size) observed in the region of about 1.2-1.5 μm. The cumulative curve shows that approximately 50 % of the particle volume (D_{50}) is accounted for by sizes of the order of 1.3-1.6 μm, while 90 % of the particles (D_{90}) are smaller than 6-8 μm. The presence of a distribution tail in the region of >10 μm indicates the presence of individual agglomerates formed during the sintering process [67]. The obtained data are in good agreement with the results of SEM analysis, confirming the formation of micron-scale agglomerates and a developed porous structure. The predominance of submicron and micron-sized particles contributes to an increase in the specific surface area and the formation of a branched pore network, which is an important factor for the adsorption and ion-exchange properties of the material. The particle size distribution demonstrates the structural heterogeneity characteristic of zeolitic aluminosilicate ceramics and confirms the potential of the Al_2SiNaO_6 composition for functional applications.

X-ray diffraction (XRD) analysis (Fig. 7) of the developed alumina-based material was performed to establish the phase composition, crystallographic parameters, and structural state of the synthesized sample.

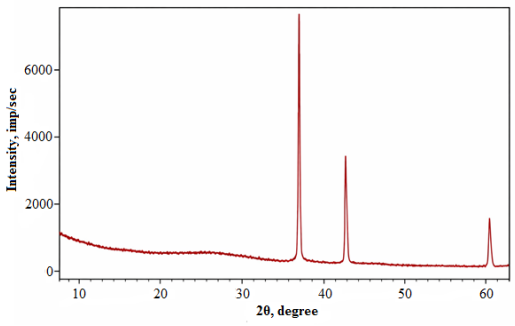

Figure 7. X-ray diffraction pattern of the developed material based on aluminum oxide [68]

The experimental X-ray diffraction pattern is characterized by a set of intense and well-resolved diffraction maxima, the position and relative intensity of which reflect the formation of a single-phase crystalline structure of the zeolite type, corresponding to sodium aluminosilicate of the composition Al_2SiNaO_6. Experimental data have shown their correspondence to the cubic syngony with the space group Fm3m. The calculated unit cell parameter is a = 4.056 nm, which is in good agreement with the literature data [69] for zeolitic aluminosilicate systems. The main diffraction maxima recorded in the X-ray diffraction pattern, as well as the corresponding interplanar distances and crystallographic indices are given in Table 3

Table 3. Diffraction maxima and calculated crystallographic parameters of the AlSiNaO-based material

№ peak	2θ, degree	θ, degree	Interplanar distance d, Å	Miller indices (hkl)	Relative intensity, %
1	38.5	19.25	2.34	(111)	100
2	44.7	22.35	2.02	(200)	~45
3	65.1	32.55	1.43	(220)	~20

The interplanar distances d_{hkl} were calculated using Bragg's law:

$$n\lambda=2d\sin\theta, \quad (2)$$

where, λ is the X-ray wavelength, θ is the diffraction angle, and n=1 is the reflection order. For a cubic crystal system, the lattice parameter was determined from the relationship:

$$a=d_{hkl}(h^2+k^2+l^2)^{1/2}. \quad (3)$$

The obtained values of the unit cell parameter, calculated from various reflections, are in good mutual agreement, indicating the correctness of the phase identification and a high degree of structural ordering. The absence of additional diffraction lines in the studied angular range is an indication of the high phase purity of the synthesized material. The content of possible impurity crystalline phases does not exceed the detection limit of the X-ray diffraction method and is estimated at less than 3-5 wt.%. Analysis of the shape of the diffraction maxima shows that the peaks are narrow and symmetrical, indicating a high degree of crystallinity and a low level of internal microstrains [70]. The sizes of the coherent scattering regions were estimated using the Scherrer formula [71]:

$$D=K\lambda/\beta\cos\theta, \quad (4)$$

where, K is the shape factor (0.9), β is the full width of the peak at half maximum.

Calculations show that the material is characterized by a finely dispersed crystalline structure typical of zeolitic aluminosilicates, which determines the developed specific surface area and potentially high sorption capacity. From a physical point of view, the formation of an ordered aluminosilicate framework with the participation of sodium ions ensures stabilization of the crystal lattice and confirms the completion of the processes of structural self-organization during synthesis [52, 54]. This is a key factor determining the material's functional properties when used in adsorption, catalytic, and ion-exchange processes. Experimental studies have shown (see Fig. 5) that porous zeolite ceramics exhibit good hydrogen absorption. For example, at a temperature of 200 °C and a pressure of 12 atm, porous aluminosilicate ceramics Al_2SiNaO_6 absorbs 11% by weight of hydrogen.

For the metals we obtained, we found that porous nickel possessed a maximum hydrogen capacity of approximately 0.7 wt.% at a pressure of 15 atm and a temperature of 300 °C, while magnesium's absorption value reached 1.5 wt.%. In the aluminum-nickel alloys, signs of hydrogenation were absent across the entire range of the studied parameters. Powdered titanium exhibited the ability to accumulate hydrogen up to 3.8 wt.% at 12 atm and 700 °C, which is slightly lower than the theoretical limit of 4.04 wt.% for TiH_2 hydride. The highest hydrogen capacity was recorded for lithium: at a temperature of 700 °C and a pressure of 12 atm, the hydrogen content reached 12.4 wt.%. According to the analysis of the obtained data, high hydrogen absorption values (over 6 wt.%) are achieved at temperatures of approximately 600-700°C and pressures above 15 atm. Metallic sodium is capable of binding up to 4.3 wt.% hydrogen [72–75].

Figure 8 shows the X-ray diffraction pattern of the original lithium metal sample before exposure to hydrogen

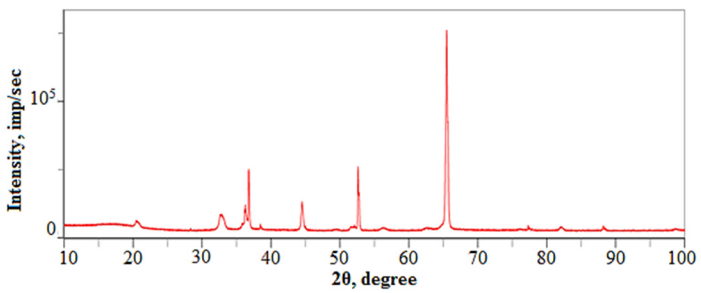

Figure 8. X-ray diffraction pattern of metallic lithium in its original state

The X-ray diffraction pattern is characterized by a set of intense and narrow diffraction peaks corresponding to metallic lithium with a body-centered cubic (BCC) lattice. The diffraction peaks and calculated physical values are listed in Table 4.

Table 4. Diffraction characteristics and interplanar distances of Li

No. peak	2θ, degree	θ, degree	Interplanar distance d, Å	Miller indices (hkl)	Note
1	36.2	18.1	2.479	(110)	The main peak of BCC lithium
2	52.3	26.15	1.748	(200)	Second reflex
3	65.1	32.55	1.432	(211)	Maximum intensity
4	77.0	38.5	1.237	(220)	Additional reflex

The main reflections were recorded at 2θ angles corresponding to the (110), (200), (211), and (220) planes, which is typical for bcc structures. The absence of additional peaks associated with lithium hydrides or oxides (LiH, Li_2O, LiOH) indicates high phase purity of the sample and minimal surface oxidation. The interplanar distances d_{hkl} were calculated using Bragg's law (2). For the most intense reflection (211) at 2θ = 65.1°, d_{211}≈1.432 Å was obtained. The cubic unit cell parameter a was calculated using formula (3), which yielded a value of 3.507 Å for the (211) reflection, which is consistent with the reference data [69] for metallic lithium at room temperature (a = 3.51 Å). The observed small width of the diffraction maxima indicates high crystallinity and large crystallites (>100 nm). The predominance of the intensity of the diffraction peak (211) compared to the reflection (110) is due to the presence of a preferred orientation of crystallites, characteristic of rolled or annealed lithium foils. In the region of small angles (10°-25°), a weak amorphous rise in the background is observed, which is associated with the presence of a thin layer of natural lithium oxide or carbonate on the surface. The absence of distinct peaks of hydrides or oxides confirms the predominance of the metallic phase in the initial state. The experimental results indicate that lithium in the initial state is a thermodynamically stable metallic phase with a well-ordered bcc lattice, ensuring high atomic mobility and the presence of interstitial positions. These properties create favorable conditions for subsequent hydrogenation and the formation of the hydride phase LiH [76-78]. The X-ray diffraction pattern confirms that the original sample is single-phase metallic lithium with a high degree of crystallinity and lattice parameters corresponding to reference data, which allows this material to be used as a reference when assessing structural changes after hydrogen treatment [79].

An X-ray diffraction pattern (Fig. 9) of metallic lithium after treatment in a hydrogen atmosphere at a pressure of 12 atm and a temperature of 700 °C allows us to evaluate the phase composition, degree of hydrogenation and structural changes of the original material.

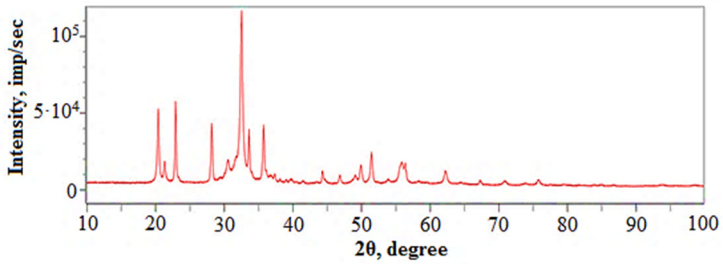

Figure 9. X-ray diffraction pattern of metallic lithium after treatment in a hydrogen atmosphere at a pressure of 12 atm and a temperature of 700°C

The diffraction pattern shows a significant weakening of the peaks of the original metallic lithium, as well as the appearance of new diffraction maxima characteristic of LiH with a cubic lattice of the NaCl type and the Fm3m space group, demonstrating partial or complete conversion of the metal into hydride under the specified conditions. Additional weak peaks in the range of 20°-35° correspond to the products of surface interaction with oxygen or moisture, such as LiOH and Li_2O [80]. The interplanar distances d_{hkl} were calculated based on Bragg's law (2). For the (111) peak of LiH at 2θ≈38.2°, the angle θ=19.1°, which gives d_{111}≈2.356 Å. The cubic lattice parameter has a value of a ≈ 4.081 Å, close to the reference value [69] for LiH (≈4.084 Å), confirming the formation of a stoichiometric hydride. The average size of the coherent scattering regions was estimated using the Scherrer formula (4). The narrow peaks of LiH indicate large crystallites (>100 nm), characteristic of hydrides obtained at high temperatures.

Table 5. Diffraction maxima and calculated parameters of LiH

No. peak	2θ, degree	θ, degree	Interplanar distance d, Å	Miller indices (hkl)	Parameter a, Å	Note
1	38.22	0.3335	2.353	(111)	4.076	Main peak LiH
2	44.39	0.3874	2.039	(200)	4.078	Second reflex
3	64.58	0.5636	1.442	(220)	4.078	Additional peak
4	77.72	0.6782	1.228	(311)	4.073	
5	81.85	0.7143	1.176	(222)	4.074	

The change in the intensity and position of the diffraction peaks compared to the original metal indicates a complete rearrangement of the lithium crystal structure. The appearance of new reflections confirms the formation of lithium hydride, and the weakening of the peaks of the original Li indicates a high degree of metal transformation. The width of the peaks demonstrates the high crystallinity of the hydride and the large sizes of the crystallites, and the increase in the background in the small-angle region indicates the presence of an amorphous phase or fine-crystalline oxidation products [81, 82]. The X-ray diffraction pattern (Fig. 9) confirms the successful synthesis of lithium hydride with a cubic structure, high crystallinity and stability of the hydride phase. The presence of additional peaks confirms the sensitivity of the material to oxygen and moisture, which form surface hydroxides and oxides. The data obtained form the basis for the analysis of the hydrogenation kinetics and thermodynamics of lithium hydrogen accumulation. In the case of lithium, the hydrogenation reaction proceeds according to the equation [80]:

$$2Li+H_2 \rightarrow 2LiH, \quad (5)$$

At an optimal temperature of 600-700 °C, the resulting lithium hydride is characterized by an ionic bond (Li^+H^-) and remains thermally stable up to its melting point of approximately 688 °C.

When heated to temperatures around 700 °C or upon contact with water, LiH decomposes, releasing hydrogen. The thermal decomposition is described by the reaction:

$$2LiH \rightarrow 2Li+H_2, \quad (6)$$

whereas when interacting with water, an exothermic reaction occurs:

$$LiH+H_2O \rightarrow LiOH+H_2. \quad (7)$$

Calculations show that up to 290 g of hydrogen can be produced from 1 kg of lithium hydride when reacted with water. Overall, it has been established that lithium, titanium, and sodium provide hydrogen storage at levels of 12.4, 4.1, and 4.3 wt.%, respectively, making these hydride systems promising for hydrogen storage and transportation.

CONCLUSIONS

In this study, porous aluminosilicate materials Al_2SiNaO_6 were synthesized based on kaolin and diatomite using burnable additives to ensure the formation of a developed porous structure. The porous ceramics of the zeolitic aluminosilicate composition Al_2SiNaO_2 are characterized by a developed hierarchical microstructure with a system of open pores of micron and submicron sizes (~0.3-2 μm). The particle sizes and their agglomerates range from 1-10 μm, while granulometric analysis revealed a polydisperse distribution with a median size of $D_{50} \approx$ 1.3-1.6 μm and a D_{90} value of < 6-8 μm. The rough surface of the grains ensures a high specific surface area for the material, ranging from 100 to 400 m²/g. The preservation of an open porous structure after heat treatment indicates an optimal sintering regime, ensuring mechanical cohesion of the framework without significant pore closure. The combination of structural characteristics suggests a high adsorption capacity of the material (~0.5-2.0 mmol/g for small molecules) and confirms the potential for the use of Al_2SiNaO_6 ceramics in adsorption, ion exchange, and catalytic processes, as well as in gas storage systems, including hydrogen storage.

X-ray diffraction analysis revealed that the samples possess a single-phase zeolite-type crystal structure with a cubic syngony and the Fm3m space group. The unit cell parameter was a = 4.056 Å, and the dimensions of the coherent scattering regions according to the Scherrer formula indicate a finely dispersed crystalline structure, which ensures a developed specific surface area and high sorption capacity.

An analysis of sorption and desorption isotherms revealed that porous Al_2SiNaO_6 ceramics at 200 °C and pressures of 1-11 atm is characterized by stepwise hydrogen absorption, reaching a maximum capacity of 10-11 wt.%. Physical adsorption occurs in the range of 1-5 atm (1-3.5 wt.%), while at 5-8 atm (up to 9-9.5 wt.%) a transition to intense mechanisms, including chemisorption and capillary condensation, is observed. Reaching a plateau at 8-11 atm reflects the saturation of the porous structure. Hysteresis in the range of 6-9 atm indicates the development of hierarchical porosity and partially irreversible processes associated with the formation of hydride phases. Desorption occurs rapidly, completing within 2 min, with the release of up to 11 wt.% hydrogen. The Al_2SiNaO_6 material has a high sorption capacity and a combined mechanism of interaction with hydrogen, demonstrating stability for up to 5 sorption-desorption cycles; after this, structural degradation is observed, limiting its cyclic stability for gas storage.

All hydrogenation experiments were conducted in a specially designed high-temperature sealed hydrogen reactor operating at pressures up to 15 atm and temperatures up to 700 °C. This reactor enabled us to achieve a high degree of hydrogenation and the stable formation of crystalline LiH. The initial lithium metal was characterized by a body-centered cubic lattice with a lattice parameter a ≈ 3.507 Å and large crystallites (>100 nm). After treatment in a hydrogen atmosphere at a pressure of 12 atm and a temperature of 700 °C, lithium was completely or partially converted to lithium hydride (LiH) with a face-centered cubic NaCl-type structure and a lattice parameter a ≈ 4.081 Å. The main interplanar distances are: $d_{111} \approx$ 2.356 Å, $d_{200} \approx$ 2.039 Å, $d_{220} \approx$ 1.442 Å, which corresponds to the reference data for LiH. The average crystallite size exceeds 100 nm, which confirms the high crystallinity of the hydride. Experimental measurements of hydrogen absorption showed maximum values: Li - 12.4 wt.%, Ti - 3.8 wt.%, Na - 4.3 wt.%, which indicates the high efficiency of lithium as a hydrogen battery at temperatures of 600-700 °C and

pressures of 12-15 atm. Lithium hydrogenation proceeds according to the equation $2Li + H_2 \rightarrow 2LiH$, and LiH maintains thermal stability up to 688 °C and can release hydrogen upon reaction with water: $LiH + H_2O \rightarrow LiOH + H_2$, yielding up to 290 g of hydrogen per 1 kg of hydride. Due to its high hydrogen capacity and stable crystalline structure under standard conditions, lithium hydride (LiH) is widely used in aerospace, portable hydrogen generators, as a neutron moderator, and as a component of fusion fuel. LiH is also a promising material for storing and transporting hydrogen in industrial processes.

Funding

The work was carried out with the financial support of the Ministry of Innovative Development of the Republic of Uzbekistan within the framework of projects AL-4821023123 "Technology of efficient storage of hydrogen in absorbed form in porous materials" and IL-9224094112 "Development of metal hydride materials and a container for storing hydrogen".

ORCID

F.A. Giyasova, https://orcid.org/0000-0003-0746-4986; **M.A. Yuldoshev,** https://orcid.org/0000-0002-9722-9439
F.A. Giyasov, https://orcid.org/0009-0003-9882-0655; **A. Egamberdiyev,** https://orcid.org/0009-0009-9653-4923
O.T. Ismanova, https://orcid.org/0000-0003-2644-2459; **S.K. Abdizhaliev,** https://orcid.org/0000-0003-1762-3645
M.A. Jalelov, https://orcid.org/0009-0001-9559-2568; **S.A. Tursinbaev,** https://orcid.org/0000-0003-4105-1843

REFERENCES

[1] Z.R. Chong, Sh.H.B. Yang, P. Babu, and P. Linga, "Review of natural gas hydrates as an energy resource: Prospects and challenges," Applied Energy, **162**, 1633-1652 (2016). https://doi.org/10.1016/j.apenergy.2014.12.061
[2] S.S. Oladosu, T.L. Amosa, T.I. Olutoki, J.O. Ansari, M.N.M. Abioye, K.J. Rehman, and Z.U Soleimani, "Hydrogen-powered horizons: transformative technologies in clean energy generation, distribution, and storage for sustainable innovation," International Journal of Hydrogen Energy, **56**, 1152-1182 (2024). https://doi.org/10.1016/j.ijhydene.2023.12.186
[3] W. Liu, J.A. Tupe, and F.A. Zinsou, "Metal Hydride Storage Systems: Approaches to Improve Their Performances," Particle & Particle Systems Characterization, **42**(3), (2024). https://doi.org/10.1002/ppsc.202400163
[4] R.A. Kerr, "Energy. Natural gas from shale bursts onto the scene," Science, **328**(5986), 1624-1626 (2010). https://doi.org/10.1126/science.328.5986.1624
[5] S.O. Akpasi, I.M.S. Anekwe, E.K. Tetteh, U.O. Amune, Sh.I. Mustapha, and S.L. Kiambi, "Hydrogen as a clean energy carrier: advancements, challenges, and its role in a sustainable energy future," Clean Energy, **9**(1), 52-88 (2025). https://doi.org/10.1093/ce/zkae112
[6] W. Gao, Z. Fu, Y. Li, Y. Li, and J. Zou, "Progress of Performance, Emission, and Technical Measures of Hydrogen Fuel Internal-Combustion Engines," Energies, **15**, 7401 (2022). https://doi.org/10.3390/en15197401
[7] S.A. Okyere, R.A. Mensah, J. Sandström, and M. Försth, "Risk and safety assessment of hydrogen pipelines and storage tanks using preliminary hazard analysis," Frontiers in Chemical Engineering, **7**, (2025). https://doi.org/10.3389/fceng.2025.1722173
[8] J. Xu, R. Wan, Xi Chen, and Binlin Dou, "Cryogenic supercritical hydrogen storage: Design and thermodynamic optimization via multi-stage Joule-Brayton refrigeration cycles," Energy, **338**, 138737 (2025). https://doi.org/10.1016/j.energy.2025.138737
[9] S.K.S. Patel, R.K. Gupta, M. Rohit, J.-K. Le, "Recent Developments in Hydrogen Production, Storage, and Transportation: Challenges, Opportunities, and Perspectives," Fire, **7**(7), 233 (2024). https://doi.org/10.3390/fire7070233
[10] N.I. Beyazit, "Comparative Study of Hydrogen Storage and Metal Hydride Systems: Future Energy Storage Solutions," Processes, **13**(5), 1506, (2025). https://doi.org/10.3390/pr13051506
[11] M. Yue, H. Lambert, E. Pahon, R. Roche, S. Jemei, and D. Hissel, "Hydrogen energy systems: A critical review of technologies, applications, trends and challenges," Renewable and Sustainable Energy Reviews, **146**, 111180 (2021). https://doi.org/10.1016/j.rser.2021.111180
[12] Y. Li, Q. Guo, Zh. Ding, H. Jiang, H. Yang, W. Du, Y. Zheng, *et al*., "MOFs-Based Materials for Solid-State Hydrogen Storage: Strategies and Perspectives," Chemical Engineering Journal, **485**(7623), 149665 (2024). https://doi.org/10.1016/j.cej.2024.149665
[13] X. Miao, J. He, H. Zhai, Zh. Wu, Y. Li, and Zh. Jin, "Adjustment the donor-acceptor COFs structure enhances the electron push-pull effect to induce electron transfer to Pt site and improve photocatalytic hydrogen evolution," Carbon, **239**, 120297 (2025). https://doi.org/10.1016/j.carbon.2025.120297
[14] S. Kumar, M. Myekhlai, S. Lim, and H. Oh, "Understanding factors affecting storage capacity and reproducibility in realistic ambient-temperature hydrogen physisorption," Sustainable Energy Fuels, **10**, 961-983 (2026). https://doi.org/10.1039/D5SE01539A
[15] P. Chen, E. Akiba, O.Sh. Ichi, A. Züttel, and L. Schlapbach, "Hydrogen Storage by Reversible Metal Hydride Formation," in: *Hydrogen Science and Engineering: Materials, Processes, Systems and Technology*, edited by P.D.D. Stolten, and D.B. Emonts, (Wiley-VCH Verlag GmbH & Co. KGaA, 2007), pp. 763-790. https://doi.org/10.1002/9783527674268.ch31
[16] S. Bagyalakshmi, A. Sivakami, R. Deeptha, G. Manikandan, T. Sukumar, and S. Srinivasulu, "MOF-Metal hydride composite materials for hydrogen storage: A comprehensive review," Journal of Alloys and Compounds, **1060**, 187192 (2026). https://doi.org/10.1016/j.jallcom.2026.187192
[17] B. Sakintuna, F.L. Darkrim, and M. Hirscher, "Metal hydride materials for solid hydrogen storage: A review," International Journal of Hydrogen Energy, **32**(9), 1121-1140 (2007). https://doi.org/10.1016/j.ijhydene.2006.11.022
[18] N. Klopčič, I. Grimmer, F. Winkler, M. Sartory, and A. Trattner, "A review on metal hydride materials for hydrogen storage," Journal of Energy Storage, **72**(Part B), 108456 (2023). https://doi.org/10.1016/j.est.2023.108456
[19] A.S. Mekonnin, K. Wacławiak, M. Humayun, Z. Shang, and H. Ullah, "Hydrogen Storage Technology, and Its Challenges: A Review," Catalysts, **15**, 260 (2025). https://doi.org/10.3390/catal15030260
[20] G. Amica, P.A. Larochette, and F.C. Gennari, "Hydrogen storage properties of $LiNH_2$-LiH system with MgH_2, CaH_2 and TiH_2 added," International Journal of Hydrogen Energy, **40**(30), 9335-9346 (2015). https://doi.org/10.1016/j.ijhydene.2015.05.091

[21] H. Hong, H. Guo, Zh. Cui, A. Ball, and B. Nie, "Structure modification of magnesium hydride for solid hydrogen storage," International Journal of Hydrogen Energy, **78**, 793-804 (2024). https://doi.org/10.1016/j.ijhydene.2024.06.327
[22] V.K. Kukkapalli, S. Kim, and S.A. Thomas, "Thermal Management Techniques in Metal Hydrides for Hydrogen Storage Applications: A Review," Energies, **16**, 3444 (2023). https://doi.org/10.3390/en16083444
[23] Sh.B. Utamuradova, F.A. Giyasova, K.N. Bakhronov, M.A. Yuldoshev, M.R. Bekchanova, and B. Ismatov, East Eur. J. Phys. (3), 325-335 (2025). https://doi.org/10.26565/2312-4334-2025-3-31
[24] S.S Kareem, Q. Hassan, H.F. Fakhruldeen, T.M. Hanoon, F.I. Jabbar, S. Algburi, and D.H. Khalaf, "A review on physical and chemical hydrogen storage methods for sustainable energy applications," Unconventional Resources, **8**, 100235 (2025). https://doi.org/10.1016/j.uncres.2025.100235
[25] W. Wang, Sh. Xu, X. Li, T. Cheng, Y. Li, W. Fang, X. Ren, and L. He, "Preparation and Hydrogen Absorption Kinetics Study of Hybrid Molding Metal Hydride Beds," Inorganics, **14**(4), (2026). 110 https://doi.org/10.3390/inorganics14040110
[26] A. Gil, R. Trujillano, M.A. Vicente, and S.A. Korili, "Hydrogen adsorption by microporous materials based on alumina-pillared clays," International Journal of Hydrogen Energy, **34**(20), 8611-8615 (2009). https://doi.org/10.1016/j.ijhydene.2009.08.057
[27] Y. Wen, X. Chai, Y. Gu, W. Wu, W. Ma, J. Zhang, and T. Zhang, "Advances in hydrogen storage materials for physical H_2 adsorption," International Journal of Hydrogen Energy, **97**, 1261-1274 (2025). https://doi.org/10.1016/j.ijhydene.2024.11.459
[28] A. Metrane, A. Delhali, M. Ouikhalfan, A.H. Assen, and Y. Belmabkhout, "Water Vapor Adsorption by Porous Materials: From Chemistry to Practical Applications," J. Chem. Eng. Data, **67**(7), 1617-1653 (2022). https://doi.org/10.1021/acs.jced.2c00145
[29] R.Ch. Muduli, and P. Kale, "Advanced materials for solid-state hydrogen storage: A review on high-surface-area innovations," International Journal of Hydrogen Energy, **170**, 151049 (2025). https://doi.org/10.1016/j.ijhydene.2025.151049
[30] M.S. Payzullakhanov, F.A. Giyasova, M.A. Yuldoshev, Ch.X. Toshpulatov, R.U. Ernazarov, F.A. Giyasov, A. Urishev, *et al*., East Eur. J. Phys. (1), 233-240 (2026). https://doi.org/10.26565/2312-4334-2026-1-25
[31] J. Matrasulov, J.R. Yusupov, and A.A. Saidov, "Fast forward evolution in heat equation: Tunable heat transport in adiabatic regime," Nanosystems: Phys. Chem. Math. **14**(4), 421–427 (2023). https://doi.org/10.17586/2220-8054-2023-14-4-421-427
[32] R.M. Ospino, A. Celzard, and V. Fierro, "Hydrogen Adsorption in High-Surface Area Porous Materials," in: *Hydrogen Storage*, (ISTE Ltd., 2025), pp. 357-393. https://doi.org/10.1002/9781394401635.ch8
[33] N.Yu. Sharibaev, A.Q. Ergashov, S.B. Fazliddinov, R.G. Ikramov, M.A. Yuldoshev, and A.A. Abdulxayev, Journal of Ovonic Research. **21**(6), (2025). https://doi.org/10.15251/JOR.2025.216.859
[34] P.K. Chauhan, R. Parameshwaran, P. Kannan, R. Madhavaram, and R. Sujith, "Hydrogen storage in porous polymer derived Silicon Oxycarbide ceramics," Ceramics International, **47**(2), 2591-2599 (2021). https://doi.org/10.1016/j.ceramint.2020.09.105
[35] M.L. Jalaluddin, U.A. Azlan, M.W. Rashid, N. Tamin, and M.N. Masri, "A review of pore-forming agents on the structures, porosities, and mechanical properties of porous ceramics," AIMS Materials Science, **11**(4), 634–665 (2024). https://doi.org/10.3934/matersci.2024033
[36] A. Mocciaro, B. Lombardi, and A.N. Scian, "Porous texture of a ceramic material made with pore formers agents," Novye ogneupory, (2017). https://doi.org/10.17073/1683-4518-2017-1-54-57 (in Russian)
[37] Lei Wang, M.Z. Quadir, and K.F. Zinsou, "Direct and reversible hydrogen storage of lithium hydride (LiH) nanoconfined in high surface area graphite," International Journal of Hydrogen Energy, **41**(40), 18088-18094 (2016). https://doi.org/10.1016/j.ijhydene.2016.07.073
[38] S. Banger, V. Nayak, and U.P. Verma, "Hydrogen storage in lithium hydride: A theoretical approach," Journal of Physics and Chemistry of Solids, **115**, 6-17 (2018). https://doi.org/10.1016/j.jpcs.2017.11.027
[39] M.G. Dadamirzaev, M.K. Uktamova, S.R. Boydedayev, M.A. Yuldoshev, and S.H. Mamadaliev, "Theoretical Analysis of Photon-Energy-Controlled Quantum Tunneling Mechanisms Based on the Landauer–Büttiker Formalism," Physics AUC, **35**, 76-84 (2025). https://share.google/EqKveBzVq9UCc2Ndc
[40] M. Abbas, D.M. Grant, M. Brunelli, and T.Ch. Hansen, "Reducing the dehydrogenation temperature of lithium hydride through alloying with germanium," Physical Chemistry Chemical Physics 15(29) (2013). https://doi.org/10.1039/c3cp51330k
[41] E. Rivard, M. Trudeau, and K. Zaghib, "Hydrogen Storage for Mobility: A Review," Materials, **12**, 1973 (2019). https://doi.org/10.3390/ma12121973
[42] T.H. Le, M.P. Kim, and Ch. Tran, "Recent Developments in Materials for Physical Hydrogen Storage: A Review," Materials, **17**, 666 (2024). https:// doi.org/10.3390/ma17030666
[43] Z. Chen, K.O. Kirlikovali, K.B. Idrees, M.C. Wasson, and O.K. Farha, "Porous materials for hydrogen storage," Chem. **8**, (2022). https://doi.org/10.1016/j.chempr.2022.01.012
[44] M.R Kalibek, A.D Ospanova, B. Suleimenova, R. Soltan, T. Orazbek, A.M Makhme, Kh.S. Rafikova, and N. Nuraje, "Solid-state hydrogen storage materials," Discov. Nano. **19**(1), 195 (2024). https://doi.org/10.1186/s11671-024-04137-y
[45] A. Alobaid, M. Kamil, and Kh.A. Khalil, "Metal hydrides for solid hydrogen storage: Experimental insights, suitability evaluation, and innovative technical considerations for stationary and mobile applications," International Journal of Hydrogen Energy, **128**(25), 432-456 (2025). https://doi.org/10.1016/j.ijhydene.2025.04.232
[46] M.S. Payzullakhanov, O.R. Parpiev, N.R. Avezova, and Zh. Shermatov, "Hydrogen Storage in Porous Ceramic Materials of Aluminosilicate Composition," Appl. Sol. Energy, **58**, 722-724 (2022). https://doi.org/10.3103/S0003701X22601338
[47] B.M. Ali, A.A. Abdulazez, G.P. Priya, S. Ray, A. Pal, R. Sharma, S. Usanov, *et al*., "Modification of graphenylene nanostructure as a promising material for adsorption and sensing of 5-fluorouracil," First-principles investigations. Journal of Molecular Graphics and Modelling, **142**, 109210 (2026). https://doi.org/10.1016/j.jmgm.2025.109210
[48] V.G. Minkina, S.I. Shabunya, V.I. Kalinin, and A. Smirnova, "Hydrogen generation from sodium borohydride solutions for stationary applications," international journal of hydrogen energy, **41**, 9227e9233 (2016). http://dx.doi.org/10.1016/j.ijhydene.2016.03.063
[49] E.P. Botella, S. Valencia, and F. Rey, "Zeolites in Adsorption Processes: State of the Art and Future Prospects," Chem. Rev. **122**(24), 17647−17695 (2022). https://doi.org/10.1021/acs.chemrev.2c00140
[50] Sh. Kumari, J. Chowdhry, M. Kumar, and M.Ch. Garg, "Zeolites in wastewater treatment: A comprehensive review on scientometric analysis, adsorption mechanisms, and future prospects," Environmental Research, **260**, 119782 (2024). https://doi.org/10.1016/j.envres.2024.119782

[51] L. Hu, W. Wu, M. Hu, L. Jiang, D. Lin, J. Wu, and K. Yang, "Double-walled Al-based MOF with large microporous specific surface area for trace benzene adsorption," Nat. Commun. **15**, 3204 (2024). https://doi.org/10.1038/s41467-024-47612-x
[52] S.F. Samadov, N.V.M. Trung, A.A. Sidorin, S.I. Ibragimova, S.H. Jabarov, M.A. Yuldoshev, *et al*., "Effect of Zn and Fe doping on vacancy cluster formation in Cu–In–Se system," Micro and Nanostructures, **209**, 208451 (2026). https://doi.org/10.1016/j.micrna.2025.208451
[53] F. Bahmanzadegan, and A. Ghaemi, "A comprehensive review on novel zeolite-based adsorbents for environmental pollutant," Journal of Hazardous Materials Advances, **17**, 100617 (2025). https://doi.org/10.1016/j.hazadv.2025.100617
[54] N. Kordala, M. Wyszkowski, and Z. Properties, "Methods of Synthesis, and Selected Applications," Molecules, **29**(5), 1069 (2024). https://doi.org/10.3390/molecules29051069
[55] F.A. Giyasova, Kh.N. Bakhronov, M.A. Yuldoshev, I.B. Sapaev, R.G. Ikramov, F.A. Giyasov, M.R. Bekchanova, *et al*., "Study of the Influence of Temperature on the Transitions of the CdS/Si/CdTe Heterosystem," East Eur. J. Phys. (4), 461-468 (2025). https://doi.org/10.26565/2312-4334-2025-4-47
[56] W.J. Roth, B. Gil, K.A. Tarach, and K.G. Marek, "Top-down engineering of zeolite porosity," Chem. Soc. Rev. **54**, 7484-7560 (2025). https://doi.org/10.1039/D5CS00319A
[57] O. Ergashev, Kh. Bakhronov, F. Giyasova, E. Nazirakhon, R. Yunusova, V. Gaffarova, O. Ochilova, *et al*., "Energy Characteristics, Adsorption Kinetics, and Mechanism of Triethylamine Adsorption on CsZSM-5 Zeolite," J. Appl. Organomet. Chem. **6**(1), 43-52 (2026). https://doi.org/10.48309/JAOC.2026.546865.1334
[58] N.S. Venkataramanan, and Y. Kawazoe, "DFT Perspective of Hydrogen Storage on Porous Materials," Materials Science, (2011). arXiv:1102.0849. https://doi.org/10.48550/arXiv.1102.0849
[59] Sh. Mirzaei, A. Ahmadpour, Z. Shao, and A.A. Niya, "Rational design of carbon-based materials for purification and storage of energy carrier gases of methane and hydrogen," Materials Science, (2022). arXiv:2204.11600. https://doi.org/10.48550/arXiv.2204.11600
[60] A. Züttel, and L. Schlapbach, "Hydrogen-storage materials for mobile applications," Nature, **414**(6861), 353-358 (2001). https://doi.org/10.1038/35104634
[61] A. Züttel, "Materials for hydrogen storage," Materials Today, **6**(9), 24-33 (2003). https://doi.org/10.1016/S1369-7021(03)00922-2
[62] J. Graetz, "New approaches to hydrogen storage," Chemical Society Reviews, **38**(1), 73-82 (2009). https://doi.org/10.1039/b718842k
[63] O.Sh. Ichi, Y. Nakamori, J.R. Eliseo, A. Züttel, and C.M. Jensen, "Complex Hydrides for Hydrogen Storage," Chemical Reviews, 107(10), 4111-4132 (2007). https://doi.org/10.1021/cr0501846
[64] M.V. Lototskyy, V.A. Yartys, B.G. Pollet, and R. Bowman, "Metal hydride hydrogen compressors: A review," International Journal of Hydrogen Energy, **39**, 5818-5851 (2014). https://doi.org/10.1016/j.ijhydene.2014.01.158
[65] M. Thommes, K. Kaneko, A. Neimark, J.P. Olivier, F.R. Reinoso, J. Rouquerol, and K.S.W. Sing, "Physisorption of gases, with special reference to the evaluation of surface area and pore size distribution (IUPAC Technical Report)," Pure and Applied Chemistry, **87**(9) (2015). https://doi.org/10.1515/pac-2014-1117
[66] B. Sakintuna, F.L. Darkrim, and M. Hirscher, "Metal hydride materials for solid hydrogen storage: A review," International Journal of Hydrogen Energy, **32**(9), 1121-1140 (2007). https://doi.org/10.1016/j.ijhydene.2006.11.022
[67] Y. Bai, G. Wagner, and Ch.B. Williams, "Effect of Particle Size Distribution on Powder Packing and Sintering in Binder Jetting Additive Manufacturing of Metals," J. Manuf. Sci. Eng. **139**(8), 081019 (2017). https://doi.org/10.1115/1.4036640
[68] M.S. Paizullakhanov, O. Parpiev, Zh.Z. Shermatov, O. Ruzimuradov, and N.N. Cherenda, "Hydrogen Absorbers Based On Porous Ceramics Synthesized In A Solar Furnace," High Temperature Material Processes An International Quarterly of High-Technology Plasma Processes, **28**(4) (2024). https://doi.org/10.1615/HighTempMatProc.2024053882
[69] J.W. Anthony, R.A. Bideaux, K.W. Bladh, and C.M. Nichols, *Handbook of Mineralogy*, (Mineralogical Society of America, 2010), pp. 4128.
[70] T. Ungár, "Microstructural parameters from X-ray diffraction peak broadening," Scripta Materialia, **51**(8), (2004). https://doi.org/10.1016/j.scriptamat.2004.05.007
[71] D. Balzar, "X-Ray Diffraction Line Broadening: Modeling and Applications to High-Tc Superconductors," J. Res. Natl. Inst. Stand. Technol. **98**(3), 321–353 (1993). https://doi.org/10.6028/jres.098.026
[72] M.S. Paizullakhanov, F.A. Giyasova, Kh.N. Bakhronov, M.A. Yuldoshev, A.A. Mamadaliev, F.A. Giyasov, F.T. Akbarova, *et al*., "Investigation of the Processes Involved in the Formation of Pyroxene Materials during Solar Melting in a Large Solar Furnace," Journal of Ovonic Research. **22**(1), 51-66 (2026). https://doi.org/10.15251/JOR.2026.221.51
[73] F.A. Giyasova, A.Z. Rakhmatov, Kh.N. Bakhronov, M.A. Yuldoshev, F.A. Giyasov, A.N. Olimov, and N.A. Sattarov, "Physical Principles of Photocurrent Generation in a Silicon-Based Photodiode Structure with a Schottky Barrier," East Eur. J. Phys. 4, 397-406 (2025). https://doi.org/10.26565/2312-4334-2025-4-38
[74] A. Tayyab, M. Shakil, N. Rehman, S.S.A. Gillani, I.A. Ahmed, and M. Kallel, "Exploring reversible hydrogen storage capacity of Li and Na metal-decorated Sc_3N_2 monolayer via DFT calculations," Journal of Energy Storage, **112**, 115489 (2025). https://doi.org/10.1016/j.est.2025.115489
[75] E. Nemukula, C.B. Mtshali, and F. Nemangwele, "Metal Hydrides for Sustainable Hydrogen Storage: A Review," International Journal of Energy Research, **2025**, 1 (2025). https://doi.org/10.1155/er/6300225
[76] S. Zhang, L. Ma, W. Liu, M. Dong, Q. Pang, Q. Li, Zh. Wu, and Xiushen Ye, "Solvent- and catalyst-free hydrogenation synthesis of lithium hydride at high altitude," Chemical Engineering Science, **295**, 120158 (2024). https://doi.org/10.1016/j.ces.2024.120158
[77] N.S.S. Singh, M.A. Rusho, A. Abilkasimov, M. Latipova, A. Aldulaimi, A.G. Taki, R.J. Albadr, *et al*., "Exploring transition metal-based electrocatalysts for carbon dioxide reduction: Towards enhanced product," Chemical Physics Letters, **880**, 142410 (2025). https://doi.org/10.1016/j.cplett.2025.142410
[78] S. Bahou, H. Labrim, M. Lakhal, and H. Ez-Zahraouy, "Improving the hydrogen storage properties of lithium hydride (LiH) by lithium vacancy defects: Ab initio calculations," Solid State Communications, **371**, 115167 (2023). https://doi.org/10.1016/j.ssc.2023.115167

[79] J.L. Snider, T.M. Mattox, Y.-S. Liu, L.F. Wan, P. Wijeratne, M.D. Allendorf, V. Stavila, *et al*., "The influence of LiH and TiH_2 on hydrogen storage in MgB2 I XPS study of surface and near-surface phenomena," International Journal of Hydrogen Energy **47**(1), 387-402 (2022). https://doi.org/10.1016/j.ijhydene.2021.09.169

[80] E. Garlea, M.O. King, E.C. Galloway, T.L. Boyd, N.R. Smyrl, H.Z. Bilheux, L.J. Santodonato, *et al*., "Identification of lithium hydride and its hydrolysis products with neutron imaging," Journal of Nuclear Materials, **485**, 147-153 (2017). https://doi.org/10.1016/j.jnucmat.2016.12.012

[81] Z.T. Azamatov, Sh.B. Utamuradova, M.A. Yuldoshev, and N.N. Bazarbaev, "Some properties of semiconductor-ferroelectric structures," East Eur. J. Phys. (2), 187-190 (2023). https://doi.org/10.26565/2312-4334-2023-2-19

[82] A. Sifuentes, A.C. Stowe, and N. Smyrl, "Determination of the role of Li_2O on the corrosion of lithium hydride," Journal of Alloys and Compounds, **580**(Supplement 1), S271-S273 (2013). https://doi.org/10.1016/j.jallcom.2013.02.046

ПОРИСТА КЕРАМІКА ТА МЕТАЛОГОДРИДНІ МАТЕРІАЛИ ДЛЯ ЕФЕКТИВНОГО ЗБЕРІГАННЯ ВОДНЮ

М.С. Пайзуллаханов[1,2], О.Р. Парпієв[1], Ф.А. Гіясова[3], С.У. Турапова[1], Е.З. Нодірматов[1], М.А. Юлдошев[4], О.Т. Ісманова[5], Ф.А. Гіясов[3], А. Егамбердієв[6], С.К. Абдіжалієв[7], М.А. Джалелов[7], С.А. Турсінбаєв[7], А.А. Абдувахобов[3]

[1]Інститут матеріалознавства Академії наук Республіки Узбекистан, Ташкент, Узбекистан

[2]Ферганський державний технічний університет, Узбекистан

[3]Міжнародний університет Кімьо в Ташкенті, Узбекистан

[4]Міжнародний університет Туран, Наманган, Узбекистан

[5]Наманганський державний університет, Наманган, Узбекистан

[6]Ташкентський інститут інженерів іригації та механізації сільського господарства, Національний дослідницький університет, Узбекистан

[7]Нукусський державний педагогічний інститут імені Аджиніяза, Нукус, Узбекистан

У цій роботі ми досліджували синтезовані пористі алюмосилікатні матеріали з вигораючими добавками, що утворюють однофазну кубічну структуру цеолітного типу (Fm3m, a = 4,056 Å). Пориста кераміка цеолітного складу за температури 200°C та тиску водню 12 атм демонструвала поглинання водню в кількості 11 мас.%. Також ми досліджували вихідний металевий літій (BCC, a≈3,507 Å), який піддавався гідрування в розробленому герметичному реакторі при 12 атм та 700 °C з утворенням гідриду LiH (FCC, типу NaCl, a ≈ 4,081 Å, d_{111} ≈ 2,356 Å). Середній розмір кристалітів LiH не перевищує 100 нм, а максимальна воднева ємність літію досягла 12,4 мас.%. Розроблений реактор дозволяє безпечно проводити гідрування за високої температури та високого тиску. Ці дані демонструють потенціал гідридів літію, титану та натрію, а також пористих алюмосилікатів для накопичення, зберігання та транспортування водню.

Ключові слова: *пористі алюмосилікати; гідрид літію; синтез; гідрування; рентгенофазовий аналіз; зберігання водню; кубічна структура; воднева ємність*